Applied Thermal Engineering 103 (2016) 807–811

Contents lists available at ScienceDirect

Applied Thermal Engineering

journal homepage: www.elsevier.com/locate/apthermeng

Biot number behaviour in the Chill Block Melt Spinning (CBMS) process

M. Pagnola [a,b,*], M. Malmoria [a], M. Barone [b]

[a] Facultad de Ingeniería, UBA, Av. Paseo Colón 850, (C1063ACV) Capital Federal, Buenos Aires, Argentina
[b] INTECIN (UBA–CONICET), Facultad de Ingeniería, UBA, Av. Paseo Colón 850, (C1063ACV) Capital Federal, Buenos Aires, Argentina

HIGHLIGHTS

- It's shown the Newtonian cooling in the thin ribbons' solidification process.
- Are studied the behaviour of the Biot number at the interfaces of the process of CBMS.
- Local vortexes that appear in the surrounding atmosphere.
- A small change in the determination of the local convection coefficient in the liquid/air interface appear.

ARTICLE INFO

Article history:
Received 28 January 2016
Revised 11 April 2016
Accepted 16 April 2016
Available online 19 April 2016

Keywords:
Chill Block Melt Spinning
Change Biot number
Newtonian cooling
Amorphous ribbons
OpenFOAM® simulation

ABSTRACT

This paper shows the change obtained in the Biot number (***Bi***) during the adhesion interface and the contact between phases, where the cooling and solidification of the ribbon obtained by the **CBMS** process occurs. This change shows an increase in the number of ***Bi*** according to the tangential velocity of the copper wheel (V_x) in the pressure range of the tests that define the ejection speeds in the nozzle (V_o).

The present study demonstrates that a zone where V_o is close to 2 m/s appears, and a transition of the $Bi_{s/l}$ numbers from magnitudes below unity until this value is exceeded can be observed.

In this study, the $Bi_{s/l} > 1$ values indicate that Newtonian cooling occurs during the ribbon's solidification process and show that the convective forces on the external part of the solidifying mass begin to influence the amount of heat transferred during the liquid/solid phase in the adhesion zone.

© 2016 Elsevier Ltd. All rights reserved.

1. Introduction

CBMS is a rapid solidification process primarily used for the production of thin metal ribbons. This process has gained wide acceptance as a means of producing amorphous and nanocrystalline materials for several technological applications in electronics [1,2].

CBMS is a complex process according to fluid dynamics, given the importance of the process parameters and their influence on the final product, regardless of the compositional variables [3].

Different mathematical models of numerical simulation have been developed to observe important characteristics of the ribbons according to the tangential speeds of the wheel (V_x), the Gap between the wheel and the nozzle (**G**), and the ejection pressure [4–6] to control the production parameters: belt width (w), thickness (t), rugosity, etc.

The Gap is a fundamental aspect of the modelling that determines the type of process used [2,7–9].

This work focuses on **G** > 1 mm and the ejection pressures on the order of 20 kPa.

The influence of the melt-spinning process variables on the structure and the physical properties of rapidly quenched alloys has been discussed in many papers and reviews [3,4,10]; it has been established that the rates of cooling in the melt-spinning process range from 4×10^4 to 5×10^6 K s^{-1} and depend mainly on the wheel velocity (V_x) [3,4,11].

In this work, V_x is placed within the mentioned ranges; therefore, we can directly relate such data to the change produced in **Bi** that relates the convective and conductive forces in the melted mass cooling process. In a physical sense, the Biot number establishes a relation between the internal conductive resistance within a solid and the external convective resistance at the solid/fluid interface. The solid state, in the studied case, is defined arbitrarily to have greater than 10^{14} kg/m s viscosity [3,13]. In analysis of one-dimensional heat conduction in simple solid bodies (large plate, long cylinder and sphere) immersed in fluids is of remarkable importance in heat transfer engineering [12]. In melt spinning

* Corresponding author at: INTECIN (UBA–CONICET), Facultad de Ingeniería, Av. Paseo Colón 850, (C1063ACV), Capital Federal, Buenos Aires, Argentina.
E-mail addresses: mpagnola@fi.uba.ar (M. Pagnola), mmalmoria@fi.uba.ar (M. Malmoria), mbarone@fi.uba.ar (M. Barone).

http://dx.doi.org/10.1016/j.applthermaleng.2016.04.077
1359-4311/© 2016 Elsevier Ltd. All rights reserved.

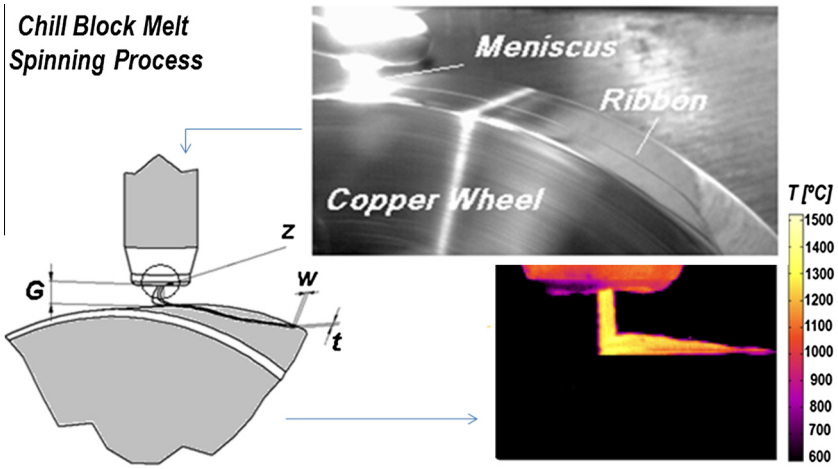

Fig. 1. CBMS process parameters.

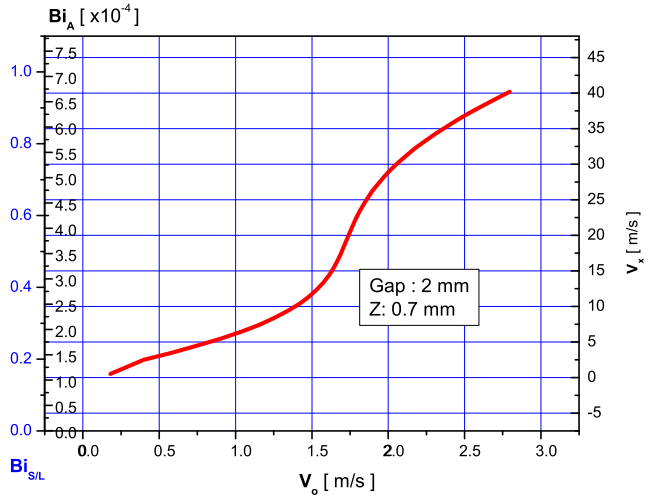

Fig. 2. Triple entrance curve for the V_o values in the nozzle that determine the ***Bi*** number according to the speed of the wheel V_x for $G = 2$ and $Z = 0.7$ mm.

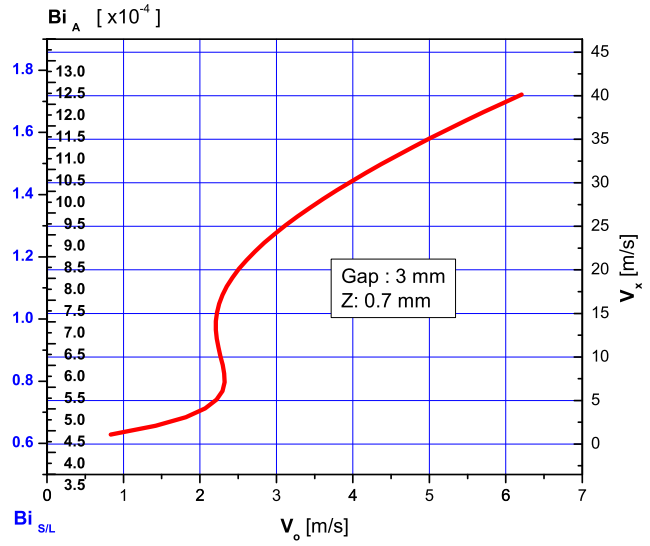

Fig. 3. Triple entrance curve for the V_o values in the nozzle that determine the ***Bi*** number according to the speed of the wheel V_x for $G = 3$ and $Z = 0.7$ mm.

process, exist a phase change liquid/solid in the final ribbon metal film obtained. Therefore there are two potential convective currents in fluids: the surrounding air and liquid fluid before phase change. For this reason there other authors using this work adopted nomenclature to de Biot number: $\mathbf{Bi_{S/l}}$ [3,9,14,15] and $\mathbf{Bi_A}$ [16].

The calculated values of the dimensionless numbers are within those obtained by other authors, enabling us to make the scheme of the present work (based on the data for the nozzle diameter values (**Z**) of 0.7 mm and Gap (**G**) values of 2, 3, and 4 mm) achieve similar results.

The result is a triple entrance curve for the values of $\boldsymbol{V_o}$ in the nozzle; the curve determines the value of ***Bi*** according to the speed ($\boldsymbol{V_x}$) of the test (see Figs. 1–3).

The values of the graphic are verified regarding their order of magnitude through a numerical simulation performed using the finite volume method at different ranges of the curve obtained ***OpenFOAM***® software and a simplified definition of the nozzle according to the gap (**G**) of the tests are used in this work.

With this model, the concordant values of $\boldsymbol{V_o}$ and $\boldsymbol{V_x}$ can be visualised.

These values define the vorticity in the contact zone, showing the influence of the coefficient of convective heat transfer (**h**) when $\mathbf{Bi_{S/l}} > 1$ and $\mathbf{Bi_A} > 7.2{\cdot}10^{-4}$.

This is indicative of Newtonian cooling in the solidification process of amorphous ribbons, the features of which are already reported in Pagnola [6,17].

2. Experimental

2.1. Obtained materials

The Mother Ingot and ribbons of amorphous material were obtained through the procedures reported in Pagnola [17].

These procedures (Fig. 1) were repeated for different tangential speeds of the copper wheel that vary from 5 to 40 m/s and for different Gaps (**G**) of 2, 3, and 4 mm. Next, the thickness (**t**) and width (***w***) values were determined:

– For the thickness (**t**), the following was used: an external micrometer (***Mitutoyo***® brand), 0–25 mm with 0.01 mm precision. Three parts of approximately 100 mm of each ribbon were selected. Next, each of those parts was measured in 10 places, and an average was obtained with the thickness values (μm).

– For the width (***w***), the following was used: a Vernier type CALIBRE (***Mitutoyo***® brand) with 0.02 mm precision. Three parts of approximately 100 mm of each ribbon were selected. Next, each of those parts was measured in 5 places, and an average was obtained with the width values (mm).

The ***t*** and ***w*** values were considered to perform the adjustments described in Pagnola [6]. The indicative temperature profile was obtained from digital image analysis as reported by Bizjan [18], for this purpose a high-speed ***Visionresearch Phantom-HD*** camera was used with a maximum pixels resolution of 640 × 480, and maximum frame rate 105.263 fps @ 32 × 16.

2.2. Data processing

With these adjustments and the equation of mass conservation [3], the following is obtained (Eq. (1)):

$$\frac{t}{w} = \frac{\pi}{4} \cdot \frac{Z}{w} \cdot \frac{V_0}{V_x} \tag{1}$$

Considering the speed range of the wheel already described, we can obtain the values of the ejection speed of the molten metal at the nozzle and correlate V_0 with V_x for Gaps of 2, 3, and 4 mm.

2.3. Biot number estimate

The estimation of the Biot number (Eq. (2)) is performed with the values of ***w*** obtained as the characteristic dimension, considering a heat-transfer coefficient (solid/liquid) in contact with the copper wheel ($h_{s/l}$) equal to 10^5 W/m^2 K [14,15]. The air heat-transfer coefficient of the rotating well is equal to 71 W/m^2 K [14], and the substrate thermal conductivity (k_{cu}) is equal to 80 W/m K [3,14]. The dimensionless Biot number is calculated by:

$$B_i = \frac{h \cdot w}{k_{cu}} \tag{2}$$

The obtained value of ***z/w*** according to the one reported in Pagnola [6] depends on the speed of the copper wheel V_x according to a decreasing exponential function for different Gaps between the wheel and the nozzle.

In the above manner, the Biot numbers ($Bi_{s/L}$ and Bi_A) can be determined according to the graphic shown in Figs. 2 and 3 for different ***G*** and ***Z*** values, showing the characteristic curves of each process.

2.4. Simulated values

OpenFOAM® software and a simplified definition of the nozzle according to the Gaps of the tests were used. For each ***G*** value, a window with the profile of the molten material can be reproduced (Figs. 5a, 6a and 7a), and another one shows the speeds involved in the simulated zone (Figs. 5b, 6b and 7b) at different points of the curves obtained (P_1; P_2; P_3 – see Fig. 4); these data are shown in Figs. 5–7 for ***G*** = 4 mm and ***Z*** = 0.7 mm.

It is possible to calculate, according to the speeds in each zone of the domain, the field of rotational speeds (*vorticity*) involved in the surrounding fluid. The case of the rotational speed of the copper wheel of 30 m/s is shown in Fig. 8.

2.5. 1D Newton's cooling law

The thermal contact between the melt (i.e., the 'puddle') and the wheel surface is quantified by a heat transfer coefficient $h_{s/l}$ defined as:

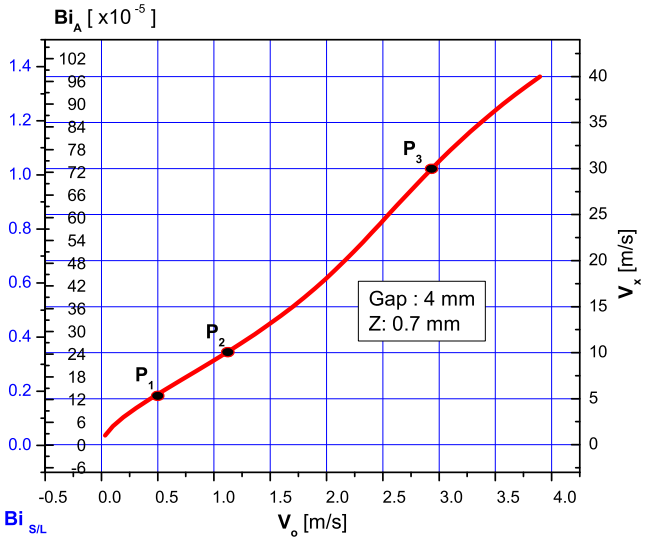

Fig. 4. Triple entrance curve for the V_o values in the nozzle that determine the ***Bi*** number according to the speed of the wheel V_x for ***G*** = 4 and ***Z*** = 0.7 mm.

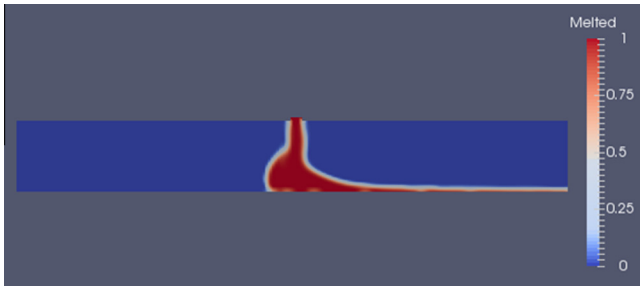

Fig. 5a. Profile of molten material in the P_1 point. Values for ***G*** = 4 mm and ***Z*** = 0.7 mm.

Fig. 5b. Simulated speeds values involved in the P_1 point. Values for ***G*** = 4 mm and ***Z*** = 0.7 mm.

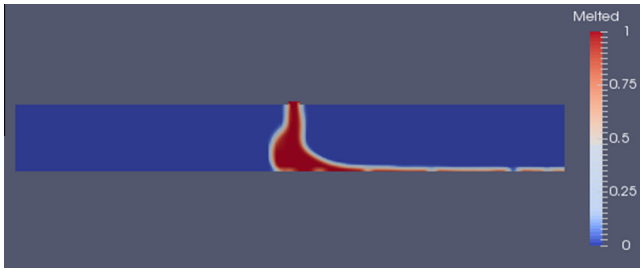

Fig. 6a. Profile of molten material in the P_2 point. Values for ***G*** = 4 mm and ***Z*** = 0.7 mm.

Fig 6b. Simulated speeds values involved in the P_2 point. Values for $G = 4$ mm and $Z = 0.7$ mm.

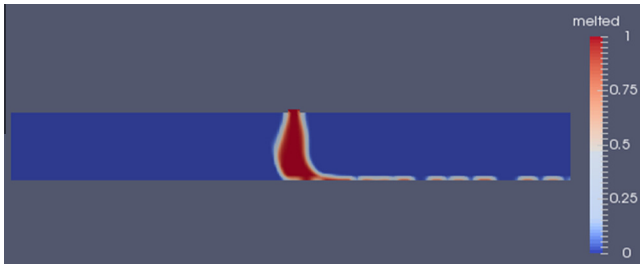

Fig. 7a. Profile of molten material in the P_3 point. Values for $G = 4$ mm and $Z = 0.7$ mm.

Fig. 7b. Simulated speeds values involved in the P_3 point. Values for $G = 4$ mm and $Z = 0.7$ mm.

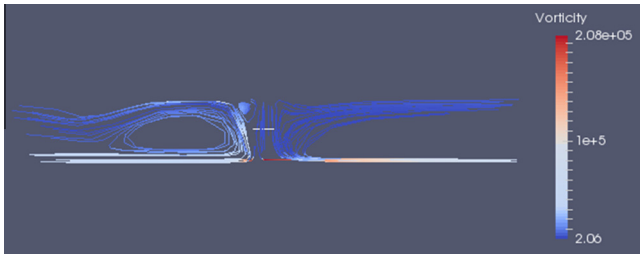

Fig. 8. P_3 values of the field of rotational speeds (vorticity) for the copper wheel speed of 30 m/s; values for $G = 4$ mm and $Z = 0.7$ mm.

$$h_{s/l} = \frac{q_w}{(T_{PB} - T_{WS})} \tag{3}$$

where q_w is the heat flux between the puddle and the wheel surface, and T_{PB} and T_{WS} are the temperatures of the puddle bottom surface and of the wheel surface, respectively [3]; q_w is given by:

$$q_w = -k_{cu} \cdot \frac{\partial T}{\partial y}; \quad (y = 0) \tag{4}$$

3. Results and discussion

3.1. General discussion

In Fig. 1, a transition zone is shown with $Bi_{s/l} < 1$ for ejection speeds V_o between 1 and 2 m/s, which defines a range of V_x between 5 and 30 m/s.

Such a zone is shown in Fig. 3 for V_o between 2 and 2.3 m/s and a smaller range of V_x between 2.5 and 15 m/s with $Bi_{s/l} < 1$.

From this point, and according to the increase in the speed, the convective forces in the external part of the solidifying mass start to increase as well, and consequently increase the $Bi_{s/l}$.

This influences the surrounding atmosphere, increasing the Bi_A to over 7.2×10^{-4}. As a result, the field of rotational speed suddenly starts the formation of local whirlwinds, which are linked to the increase in the convective forces, as reflected in the illustrated Bi_A.

This transition disappears when the Gap increases between the wheel and the nozzle, as visualised in P_3 in Fig. 4, where the vorticity begins as a speed of over 30 m/s because, at that speed, local vortices appear in the surrounding atmosphere at speeds in the range of 12–14 m/s (Fig. 7), i.e., 6–7 times the value of V_o.

This situation does not occur for P_1 and P_2 because they do not show large local vortices as they have speeds under 2.5 and 5 m/s, respectively, and are comparable to V_o (see Figs. 5b and 6b), corresponding to $Bi_{s/l} < 1$.

3.2. Particular discussion

During the initial stage of the melt touching the wheel surface, the melt is just ejected from the nozzle slit and there is no circulating flow in the melt. When the upstream and downstream menisci have moved appreciably away from the slit boundary, two circulating flows are formed in the melt below the crucible walls; this causes a nonuniform temperature distribution in the melt [16]. The appearance of local vortices in the atmosphere surrounding the solidifying metal jet increases the convective flow, which leads to the air flowing along the wheel surface, forming a large zone recirculation as demonstrated in simulation (Fig. 8). This process is seen in the increase of Bi_A, indicating that q_w must be corrected by effect of the local convection in the liquid/air interface as a result of the increased local vorticity.

Such a small correction is given by Eq. (5) as this will decrease the q_w effect in Eq. (6):

$$q^* = h_A \cdot (T_m - T_A) \tag{5}$$

where:

h_A: 71 W m^{-2}/K, according Liu et al. [16].
T_m–T_{PB}: Temperature (K).
T_A: Surrounding air temperature (K).

Thus, (Eq. (3)) of Newtonian cooling in contact zone is modified as follows:

$$h_{s/l} = \frac{q_w - q^*}{(T_{PB} - T_{WS})} \tag{6}$$

This result is according to a decrease in the heat-transfer coefficient that is established during the different rotation cycles [16], with the increase in wheel temperature in real process and the temperature distribution in the melt [18] (see Fig. 1).

4. Conclusions

Various **CBMS** tests were performed via the rapid solidification technique to characterise the Biot number in the intervening

interfaces with different ejection conditions. We observed that for $Bi_{s/l} > 1$ and $Bi_A > 7.2 \cdot 10^{-4}$, the process of convective heat transmission is influenced, and in Newtonian cooling, indicative vorticidade appear. This result indicates that the coefficient calculations are modified according to the dimensional expression described in Eq. (6). The correction q^* that should be made for a mass of molten metal at $T_m = 1600$ K and the simulated nozzle of $Z = 0.7$ mm with a $G = 4$ mm is comparable to that of a 60 W light bulb.

Such value for the calculated constant $h_{s/l}$ [3,9,14] represents an error in ±0.0461 W m^2/K in the suggested Newtonian dimensional model.

In addition, in Figs. 1 and 2, a transition is observed at $Bi_{s/l} > 1$, with a profile of ejection speeds V_o that plateaus for $G = 2$ and $G = 3$ mm. This situation does not occur with $G = 4$ mm, where the variation of $Bi_{s/l}$ and Bi_A is more gradual and without visible plateaus in V_o. This phenomenon might be attributed to vorticity decrease in the surrounding air with high gaps, and that the process starts to be controlled via ejection velocity, not by pressure as generally occurs with smaller gaps.

Acknowledgements

The authors of this paper are grateful to Dr. Andrés Guillermo Marrugo Hernández by set up parameters ***Visionresearch Phantom-HD*** camera; to CONICET – Argentina and ANPCyT – Argentina (FS Nano 03/10 program) for funding the present research.

Appendix A. Supplementary material

Supplementary data associated with this article can be found, in the online version, at http://dx.doi.org/10.1016/j.applthermaleng.2016.04.077.

References

[1] P.H. Steen, C. Karcher, Fluid mechanics of spin casting of metals, Annu. Rev. Fluid Mech. 29 (1997) 373–397, http://dx.doi.org/10.1146/annurev.fluid.29.1.373.
[2] D. Pavuna, Production of metallic glass ribbons by the chill-block melt spinning technique in stabilized laboratory conditions, J. Mater. Sci. 16 (1981) 2419–2433.
[3] C. Wang, Numerical modeling of free surface and rapid solidification for simulation and analysis of melt spinning, Iowa State University, Ames Ed., Pro Quest, UMI Dissertation Publishing, 2010, pp. 1–138 (ISBN 10: 1243778733/1-243-77873-3).
[4] V.I. Tkatch, A.I. Limanovski, S.N. Denisenko, S.G. Rassolov, The effect of the melt-spinning processing parameters on the rate of cooling, Mater. Sci. Eng., A 323 (2002) 91–96.
[5] F. Muller, US patent no 4199117, 1980.
[6] M. Pagnola, M. Barone, M. Malmoria, H. Sirkin, Influence of z/w relation in Chill Block Melt Spinning (CBMS) process and analysis of thickness in ribbons, Multidisc. Model. Mater. Struct. 11 (1) (2015) 23–31.
[7] R. Dhadwal, Numerical simulation of two-phase melt spinning model, Appl. Math. Model. 35 (6) (2011) 2959–2971.
[8] M. Bussman, J. Mostaghimi, D.W. Kirk, J.W. Graydon, A numerical study of steady flow and temperature field within a melt spinning puddle, Int. J. Heat Mass Transf. 45 (19) (2002) 3997–4010.
[9] T. Praisner, J.S.J. Chen, A. Tseng, An experimental study of process behaviour in planar flow melt spinning, Metall. Mater. Trans. B 26 (1) (1995) 1199–1208.
[10] G. Pozo Lopez, L.M. Fabietti, A.M. Condo, S.E. Urreta, Microstructure and soft magnetic properties of Finemet-type ribbons obtained by twin-roller melt-spinning, J. Magn. Magn. Mater. 322 (2010) 3088–3093.
[11] B. Karpe, B. Kosec, M. Bizjak, Analyses of the melt cooling rate in the melt-spinning process, J. Achiev. Mater. Manuf. Eng. 51 (2) (2012) 59–65.
[12] A. Campo, J.Y. Chang, Facile prediction of total heat transfer from simple solid bodies to neighboring fluids: a viable alternative to Gröber charts, Appl. Therm. Eng. 75 (2015) 541–546.
[13] W. Kurz, D.J. Fisher, Fundamentals of Solidifications, Trans Tech Publication Ltd, Switzerland, 1998.
[14] J.K. Carpenter, Heat transfer and solidification in planar-flow melt-spinning high wheel speeds, Int. J. Heat Mass Transf. 40 (9) (1997) 1993–2007.
[15] S.L. Wu, C.W. Chen, W.S. Hwang, C.C. Yang, Analysis for melt puddle in the planar flow casting process – a mathematical modelling study, Appl. Math. Model. 16 (1992) 394–403.
[16] H. Liu, W. Chen, S. Qiu, G. Liu, Numerical simulation of initial development of fluid flow and heat transfer in planar flow casting, Metall. Mater. Trans. B 40 (3) (2009) 411–429.
[17] M. Pagnola, M. Malmoria, M. Barone, H. Sirkin, Analysis of $Fe_{78}Si_9B_{13}$ (%at.) ribbons of noncommercial scrap materials produced by melt spinning equipment, Multidisc. Model. Mater. Struct. 10 (4) (2014) 511–524.
[18] B. Bizjan, B. Širok, J. Drnovšek, I. Pušnik, Temperature measurement of mineral melt by means of a high-speed camera, Appl. Opt. 54 (26) (2015) 7978–7984.